Hindawi
Shock and Vibration
Volume 2021, Article ID 5581455, 17 pages
https://doi.org/10.1155/2021/5581455

Research Article

Research on Multiobjective Optimization of Bulb Tubular Turbine Based on Orthogonal Test

Jie Sun[1], **Ye Zhou**[2], **Xinfeng Ge**[1], **Jianguo Cai**[3], **Yang Han**[3], **Hui Zhang**[3], **Jinliang Wang**[4], **Lei Zhang**[5], **Dong Chen**[1], **Hongchang Hua**[1], **Li Li**[1] and **Yuan Zheng**[1]

[1]*Hohai University, Nanjing 210098, Jiangsu Province, China*
[2]*China Institute of Water Resources and Hydropower Research, Beijing 100038, China*
[3]*Chongqing Shipping Construction Development Co., Ltd., Chongqing 500000, China*
[4]*Huanghe Wanjiazhai Hydro Junction Co., Ltd., Pianguan, Shanxi 036412, China*
[5]*Yellow River Institute of Hydraulic Research, Zhengzhou 450003, China*

Correspondence should be addressed to Xinfeng Ge; gexinfeng@hhu.edu.cn

Received 31 January 2021; Revised 23 March 2021; Accepted 19 April 2021; Published 29 April 2021

Academic Editor: Ling Zhou

The bulb tubular unit has advantages over other units in the low head, large discharge, and tidal energy. The development and utilization of low head and ultralow head hydraulic resources can increase the runner's energy parameters, make up for the defects of large size and low speed of the unit, and reduce the construction investment. The bulb tubular turbine's operation stability and structural strength are compared and analyzed by the orthogonal test method to improve the perfomance of bulb tubular turbine. The results show that the optimal design scheme can be obtained when the number of guide vane is 16, the distance between the guide vane and the blade is 1995 mm, the hub ratio is 0.31, the relative twist angle of the blade is 27°, and the cascade density is 0.72. After optimization, the bulb tubular turbine's efficiency and output are increased by 5.72% and 2.86% at a low flow rate, respectively. The vortex at the tailpipe is reduced, and the blade work effect and the cavitation performance are well. The maximum pressure pulsation amplitude in the flow passage is reduced by 73.15%, the maximum blade deformation is reduced by 39.59%, and the maximum blade static stress is reduced by 13.16%. Finally, the reliability of numerical simulation results is verified by the model test.

1. Introduction

Tubular turbines have been widely used and developed rapidly due to their excellent technical and economic characteristics and applicability since they came out in the 1930s. Tubular turbine technology, including bulb tubular generator, has become increasingly mature. The development, design, operation technology, and experience of the tubular hydropower stations are becoming more abundant [1]. Since the construction of the bulb tubular turbine in the late 1970s, bulb tubular turbines have accounted for nearly 30% of hydropower. However, with the increase in the operation of bulb tubular turbine units, the problem of failure is gradually exposed by the unit's operation [2, 3]. It wastes hydraulic resources and reduces the unit's operating efficiency, resulting in the reduction of economic benefits, and there are great safety hazards in the operation of the unit [4]. Moreover, the guide vane and runner section's design parameters will affect the structural strength of the flow passage components, the hydraulic performance, and the stability of the unit [5]. Therefore, choosing reasonable design parameters has an important impact on hydropower stations' economic operation and investment.

The development of CFD has brought great convenience to the design and optimization analysis of hydraulic machinery [6–9]. Wang et al. [10] obtained the influence law of the tubular turbine runner cascade density on the turbine's hydraulic efficiency through theoretical analysis and experimental research. Zhao et al. [11] established different blade models by changing the shape and position of the

blade inlet and outlet sides. They used ANSYS-Bladegen to conduct a numerical simulation study on the bulb tubular turbine unit with C-type blades and S-type blades and summed up the flow characteristics and energy characteristics of the different type blade unit. Yang et al. [12] considered the runner blades as a spline surface with coordinate sets when optimizing the bulb tubular turbine's runner blades. By changing the control points' angle, the blade geometric parameters were modified, making the optimization design simple and easy. Li et al. [13] optimized the operating conditions from the perspective of energy to obtain the guide vanes' optimal characteristic area under different operating conditions, which improved the operating efficiency and stability of the unit. Zhang et al. [3] reduced the unit fluctuation and improved the efficiency and output by optimizing the unit coordination curve. Wang et al. [5] studied the effect of blade opening and guide vane opening on each flow-through component's hydraulic loss. They found that the hydraulic loss of the guide vane section and runner section accounted for a large proportion, which provides reference opinions for the bulb tubular turbine's optimization design. Li et al. [14] studied the joint flow performance between the blades and guide vanes of the designed turbine unit through joint numerical simulation, which laid the foundation for studying the optimal matching relationship between the blades and guide vanes. Zheng et al. [15] optimized the bulb tubular unit without movable guide vanes under microhead conditions by adding different guide vane support methods and guide vane widths. Kim et al. [16] and Kang et al. [17] focused on the influence of different guide vane openings on bulb tubular turbines from the perspective of hydraulic performance and cavitation performance.

Most of the above studies carried out structural optimization by changing a certain design parameter (guide vane or runner), while few studies on structural optimization by changing multiple design parameters were carried out. This paper uses the orthogonal test method to optimize the bulb tubular turbine to improve the bulb tubular turbine's overall optimization level, and find out the main geometric parameters that affect the performance of the bulb tubular turbine device. Based on the L_{16} (4^5) orthogonal table, 16 sets of schemes are obtained. The in-depth study on the number of guide vanes, the distance between the guide vanes and the blades, the ratio of the hub part of the runner, the relative twist angle of the blades, and the density of the cascade density on the bulb flow was carried out. The five evaluation indexes' influence rules, such as the efficiency, output, pressure pulsation, blade deformation, and blade static stress of the hydraulic turbine, were determined by a comprehensive frequency analysis method. The performance of the unit before and after optimization was compared and analyzed.

2. Orthogonal Test Theory

The orthogonal test method is an efficient test design method based on the basic principles of probability theory and mathematical statistics [18, 19]. This method makes intensive optimization work easy and fast, and it has been widely used in various fields such as industry, medicine, chemical industry, scientific research, military, economics, and construction [20]. In recent years, the orthogonal test method is also widely used in the design and optimization of hydraulic machinery [21].

In orthogonal experimental design, the test index, test level, and the test factors are the parameters that need to be carefully considered. The test index can judge the test result, the test factor is the crucial variable in the experiment process, and the test level represents the different states of the test factors [22].

The orthogonal test table is the core of the orthogonal test method's essential analysis tool [14]. After research by Japanese scientist Taguchi, orthogonal tables have formed a normative use. In this paper, an orthogonal table L_{16} (4^5) with five factors and four levels is selected to optimize the turbine's design [23].

3. Orthogonal Test Plan Design

3.1. Investigation Indicators and Test Purpose. The purpose of the test is to improve the hydraulic performance and operating stability of the bulb tubular turbine unit, and ensure the flow components' structural strength. Five evaluation indexes are selected: efficiency, output, pressure pulsation, blade deformation, and blade static stress.

3.2. Determine Test Factors and Levels. According to the structural design requirements of the bulb tubular turbine, the number of guide vanes (factor A), the distance between the guide vanes and blades (factor B), the hub ratio (factor C), the relative twist angle of the blades (factor D), and cascade density (factor E) have a significant impact on the performance of the unit. Therefore, they are selected for this test to optimize the orthogonal test.

3.2.1. Number of Guide Vanes Z0. The conical guide vane in the bulb tubular turbine meets the requirement of the required amount of circulation in front of the runner and must meet the requirement of closing and sealing. The number of original guide vanes is 14, and the number of guide vanes of large-sized and medium-sized tubular turbines is usually 12, 16, and 20 [24]. The number of runner blades is 3, if the number of guide vanes is 12 and 15, there will be easy to cause unit resonance. The final selection of the number of guide vanes Z0 = 14, 16, 17, 20.

3.2.2. Distance between Guide Vane and Blade L1. The distance between the guide vane and the blade is defined as L1, and its value is generally (0.65 ~ 0.8) D1 [24]. This distance has a significant effect on the energy characteristics of the hydraulic unit device. In this orthogonal test, the diameters of the runner were selected as 0.6D1, 0.65D1, 0.7D1, and 0.75D1, that is, L1 = 1710, 1852.5, 1995, 2137.5 mm. Figure 1 is a schematic diagram of the distance between different guide vanes and blades.

3.2.3. Hub Ratio d. The hub ratio of the runner is an important design parameter in the bulb tubular turbine. It is related to the arrangement of the blade operating mechanism and has a great impact on the hydraulic performance of the turbine and the structural rigidity of the runner. This article mainly studies the influence of the change of the runner's hub ratio on the performance of the hydraulic turbine. The calculation method of the runner hub ratio is shown in formula (1). The original hub ratio is 0.33. This paper chooses the hub ratio $d = 0.29$, 0.31, 0.33, 0.35 for research. The schematic diagrams of different hub ratios are shown in Figure 2:

$$d = \frac{\text{hub diameter } d_B}{\text{rim diameter } D_1}. \quad (1)$$

3.2.4. Relative Twist Angle of Blade $\Delta\beta 0$. The relative twist angle of the blade affects the overflow when the unit is running. For the tubular turbine runner, the blade's optimal relative twist angle is $18^\circ \sim 28^\circ$ [24]. The relative twist angle of the original blade is 23.5°, and the relative twist angle of the blade is 20°, 23.5°, 27°, and 30.5°. Figure 3 is a schematic diagram of blade relative twist angle.

3.2.5. The Cascade Density l/t. The cascade density is an essential parameter in the design of the runner. Its value not only affects the runner's flow but also affects the runner's cavitation performance and hydraulic stability. The density of the hub cascade is generally 1.3 to 1.4 times that of the rim cascade. When the number of blades is 3, the rim cascade's density ranges from 0.75 to 0.85 [25]. When the number of blades is determined, the cascade density is mainly determined by the chord length, and the blade cascade density is changed by modifying the chord length. The original cascade density at the rim is 0.84. The rim cascade density is set to 0.72, 0.76, 0.80, and 0.84 during the process of structural optimization. Figure 4 is a schematic diagram of the cascade density at the blade rim.

3.3. Making Orthogonal Test Table. A, B, C, D, and E are used to denote five test factors, and each factor has four levels. According to the orthogonal test principle, an L_{16} (4^5) orthogonal table is shown in Table 1.

4. Numerical Simulation Calculation Settings and Experimental Verification

4.1. Three-Dimensional Model of Hydraulic Turbine. This article takes a three-blade bulb tubular turbine as the research object. The main design parameters of the turbine model are shown in Table 2.

UG NX is used to model the bulb tubular unit, which is mainly divided into four parts: the inlet flow channel section, the guide vane section, the runner section, and the draft tube section, as shown in Figure 5.

4.2. Meshing. ICEM is used to divide the grid of fluid computation domain. Mesh division is the basic way to realize regional discretization in computational fluid dynamics. The quality and quantity of the mesh division will affect the calculation time and calculation accuracy. The unit's complex structure is divided by an unstructured grid with good adaptability, and the mesh of critical parts is locally refined [26]. Different numbers of grids are divided to verify the grid's independence, as shown in Table 3.

The results of Table 3 show that when the grid reaches a certain number, the increase of cell number has little effect on the numerical simulation results, and the relative error of efficiency is within 0.1%. Therefore, it is finally determined that the cell number of grids for the entire flow channel was about 5.7 million. The mesh division of the guide vane section and runner section is shown in Figure 6.

The solid computing domain includes the hub and blades of the runner chamber. Using the mesh module in ANSYS Workbench, the solid computing domain is discreted. The tetrahedral mesh is selected, with a grid size of 30 mm. It is found that when the number of grid cells is changing, the maximum displacement value changes very little, but the maximum stress value differs greatly. This is because the blade root is prone to stress concentration and the gradient of stress change is large [27]. With the continuous refinement of the grid at the stress concentration, the maximum static stress will reach a convergence value, as shown in Table 4. When the cell size is 10 mm after refining three times at the stress concentration location, the calculation value converges.

4.3. Boundary Condition Setting. The settings of the flow field's boundary conditions are as follows: the numerical simulation calculation is carried out on the ANSYS CFX code. The RNG k-ε turbulence calculation model is selected, and the y+ value near the wall is guaranteed ($30 < y+ < 100$). Assuming that the wall is a non-sliding wall, the pressure inlet is selected as the inlet boundary, and the free outflow is selected as the outlet boundary. The calculation accuracy of CFX is set to 10-5. When the calculated head and efficiency change is less than 1%, the calculation is considered convergent.

In the steady calculation, the dynamic and static interface is set to the frozen rotor type. In the unsteady calculation, the dynamic and static interface is set to the transient frozen rotor type. The interface grid is set as a GGI connection to ensure the transmission of energy on both sides of the interface. In the unsteady calculation, the

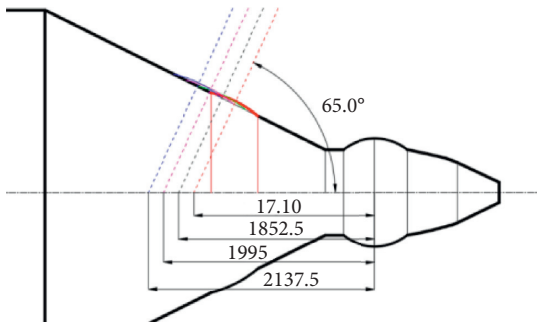

Figure 1: Schematic diagram of the distance between guide vane and blade.

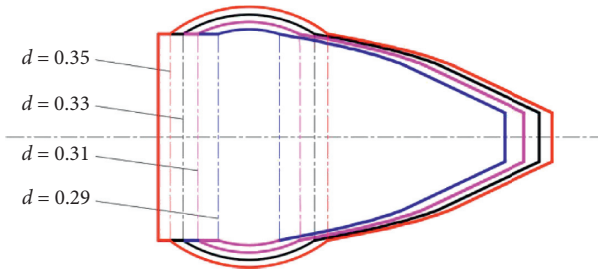

Figure 2: Schematic diagram of the hub ratio of the runner.

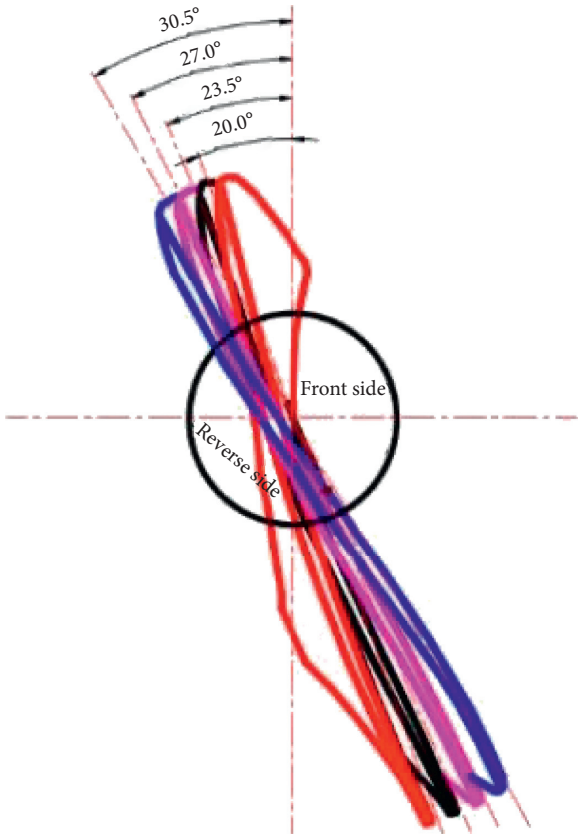

Figure 3: Schematic diagram of blade relative torsion angle.

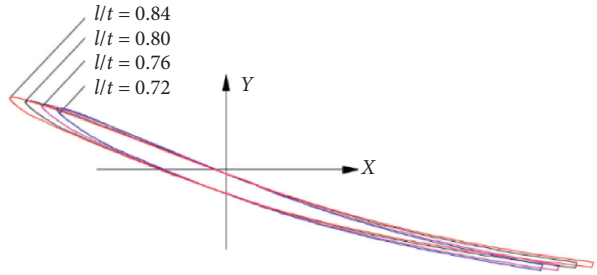

Figure 4: Schematic diagram of the density of the cascade at the blade rim.

rotation period T is 0.4 s, so the time step is set as $\Delta t = 0.00333$ s (the time required for every 3°revolutions of the runner). The first six rotation periods are selected for the calculation. Some monitoring points are set at the guide vane inlet, runner inlet, runner outlet, and draft tube to obtain information on the pressure pulsation in the turbine's interior during operation. The layout of the monitoring points is shown in Figure 7, and the monitoring points are evenly arranged from runner hub to rim.

The boundary conditions of the structural field are set as follows: (1) apply fixed constraints to the cylindrical surface of the hub shaft; (2) apply gravity and rotation constraints; (3) load water pressure on the fluid-solid coupling surface [28], as shown in Figure 8 is shown.

4.4. Model Test Verification

4.4.1. Test Device. In order to verify the reliability of the numerical simulation in this paper, a model test of the optimized hydraulic turbine was carried out on a multifunctional hydraulic test rig. The test rig is designed and constructed in accordance with China's water conservancy industry standards. The comprehensive accuracy of the multifunctional hydraulic test rig is ±0.35% (level A) accuracy. Figures 9 and 10 are schematic diagrams of the three-dimensional model of the test rig and the photo of the multifunctional test rig, respectively.

During the experiment, the model turbine's assembly and testing are strictly in accordance with the relevant regulations of the Turbine Model Acceptance Test Regulations (DL 446-91). After ensuring that the model turbine is running for a while and the water flow is gradually stabilized, the external characteristic parameters are measured and improve the accuracy of the measurement.

4.4.2. Analysis of Results. The model test mainly measures and calculates the efficiency of the unit. The size of the whole flow passage of the model turbine is geometrically similar to that of the prototype turbine, and the diameter of the runner of the model turbine is 0.38 m. In the test, six working conditions with increasing flow rates are selected, and the specific parameters are shown in Table 5.

It can be seen from Table 5 that the efficiency value obtained by the hydraulic turbine model test is lower than the efficiency value calculated by numerical simulation because of the friction and mechanical loss of the blade and the runner, bearing, coupling, and other parts during the model test. Simultaneously, there exists the blade assembly position deviation between the model test and the numerical simulation. For small flow conditions, the characteristics of water flow turbulence in the flow passage are obvious, and the velocity fluctuation is also large. This leads to large fluctuations in the measured values of flow, torque, and speed during the model test of small flow conditions, resulting in a small flow model test, and the error of numerical simulation is too large. The maximum error between the model test value and the numerical simulation calculation value is ±3%, verifying the reliability of the numerical calculation model and method in this paper.

5. Analysis of Optimization Plan

5.1. Numerical Calculation Results. Under the turbine's rated operating conditions, 16 sets of schemes are subjected to steady, unsteady, and unidirectional fluid-solid coupling calculations, and the calculation results are analyzed. The operating efficiency and output of the units under each scheme are obtained through the steady flow calculation. The time-domain information of pressure pulsation is obtained through unsteady calculation, and the frequency domain characteristics are obtained through Fourier transform. The maximum static stress and maximum deformation of the runner blade under various design schemes are obtained through the unidirectional fluid-solid coupling calculation. Table 6 is the calculation result of each scheme. Among them, the pressure pulsation coefficient C_p [29] is as follows:

$$C_P = \frac{\Delta H}{H} \times 100\%, \tag{2}$$

where ΔH is the head pulsation value, m; H is the calculated head, m.

5.2. Intuitive Analysis. After intuitive analysis of the calculation results of 16 schemes, the better schemes were obtained as (a), (b), (c), (d), and (e), as shown in Table 7.

5.3. Range Analysis. By calculating the range value, the weight of each factor level's influence on each index can be obtained. The larger the range value is, the greater the influence weight of the selected level on the test index under

Table 1: Orthogonal test plan.

Test plan	Experimental factors				
	Number of guide vanes Z_0 (A)	Distance between guide vane and blade $L1$ (B)/mm	Hub ratio d (C)	Relative twist angle of blade $\triangle\beta_0$ (D)/°	Cascade solidity l/t (E)
1	14	1710	0.29	20	0.72
2	14	1852.5	0.31	23.5	0.76
3	14	1995	0.33	27	0.80
4	14	2137.5	0.35	30.5	0.84
5	16	1710	0.31	27	0.84
6	16	1852.5	0.29	30.5	0.80
7	16	1995	0.35	20	0.76
8	16	2137.5	0.33	23.5	0.72
9	17	1710	0.33	30.5	0.76
10	17	1852.5	0.35	27	0.72
11	17	1995	0.29	23.5	0.84
12	17	2137.5	0.31	20	0.80
13	20	1710	0.35	23.5	0.80
14	20	1852.5	0.33	20	0.84
15	20	1995	0.31	30.5	0.72
16	20	2137.5	0.29	27	0.76

Table 2: Basic parameters of bulb tubular turbine.

Number	Basic parameters	Numerical value	Units
1	Runner diameter	2.85	m
2	Nominal output	3000	kW
4	Rated head	5.2	m
5	Minimum head	3.5	m
6	Rated speed	150	r/min
7	Rated flow	64.83	m^3/s

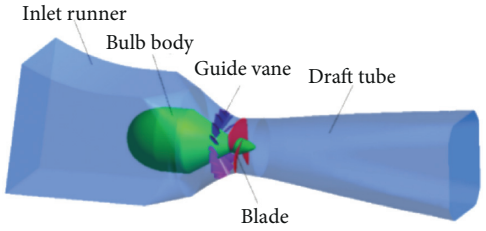

Figure 5: Model diagram of bulb tubular.

Table 3: Grid number and unit efficiency.

Case	Cell numbers	Efficiency/%
1	4.4 million	88.9
2	4.8 million	89.7
3	5.2 million	90.2
4	5.6 million	90.8
5	6.0 million	90.9

this factor is. The influence of indicators is shown in Figure 11.

Based on the data of range analysis and the relationship between each factor level and the index, an in-depth analysis of each factor level's impact on the index under rated conditions is performed. An optimal plan under the range analysis is determined.

5.3.1. Influence of Guide Vane Number Z0 (Factor A). The water guide mechanism is an essential part of the hydraulic turbine. The number of guide vanes Z0 involves its own processing volume and economic investment and affects the uniformity of the water flow into the runner. It can be seen from Figure 11 that with the increase of the number of guide vanes, the efficiency and output of the unit increase first and

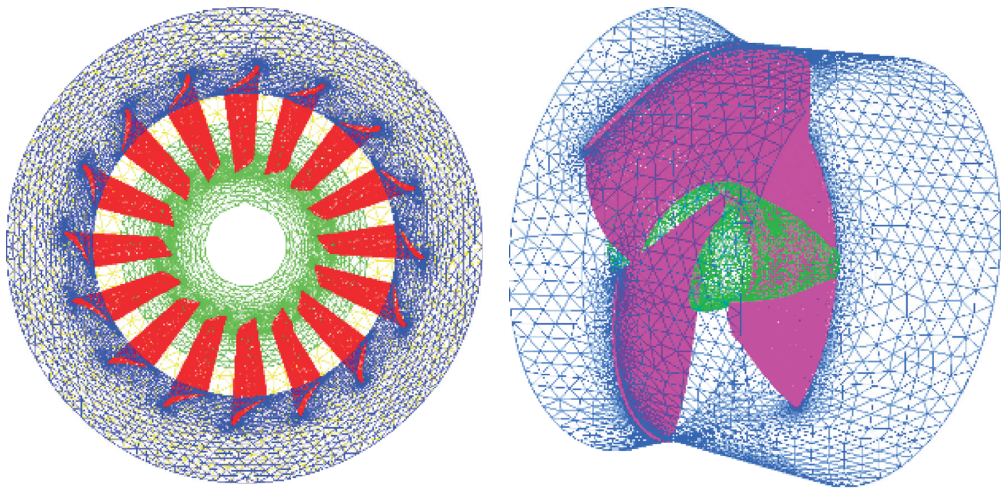

(a) (b)

Figure 6: Mesh division: (a) guide vane section; (b) runner section.

Table 4: Grid division of solid computing domain.

Meshing scheme	Units	Number of nodes	Maximum stress value/MPa	Maximum displacement value/mm
30 mm	8568	16244	14.11	1.54
20 mm	23007	39932	15.78	1.56
10 mm	188415	291972	19.24	1.62
Refined 1 time	223936	341825	20.06	1.62
Refined 2 times	315840	471858	20.24	1.62
Refined 3 times	430935	626276	20.25	1.62

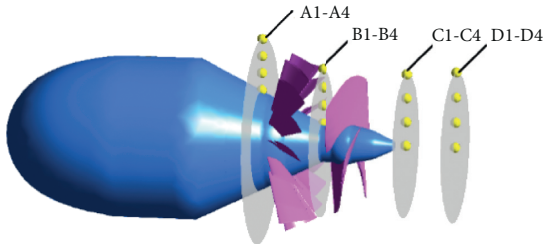

Figure 7: Layout of monitoring points.

then decrease. The change of the number of guide vanes has no obvious influence on the pressure pulsation coefficient and blade deformation. When $Z0 = 16$, the unit's efficiency and output are the largest, but the pressure pulsation coefficient, blade deformation, and static stress value are relatively high. The following conclusions can be concluded: when the number of guide vane is small, the flow into the runner is not uniform, which affects the energy conversion. When the number of guide vane is large, the flow area decreases and the exclusion coefficient increases, which affects the unit efficiency and output.

5.3.2. The Influence of the Distance L1 between the Guide Vane and the Blade (Factor B). It can be seen from Figure 11 that when distance L_1 between the guide vane and the blade gradually increases from $0.60D_1 \longrightarrow 0.65D_1 \longrightarrow 0.70D_1 \longrightarrow 0.75D_1$, the operating efficiency of the unit increases first and then decreases, and the output gradually increases. When L_1 is large, the hydraulic performance of the unit is well; the change of L1 has no obvious effect on the pressure pulsation coefficient, but when $L_1 = 0.75D_1$, the pressure pulsation coefficient is the smallest; with the increase of L_1, the maximum deformation of the blade decreases first and then increases. When $L_1 = 0.70D_1$, the blade deformation is the minimum. When $L_1 > 0.60D_1$, the blade's maximum static stress does not change with the change of L_1. The larger the distance between the guide vane and the blade is, the more stable and uniform the water flow into the runner is, and the hydraulic performance is improved to some extent. However, when the distance is too large, the flow circulation in front of the runner will be weakened, weakening the

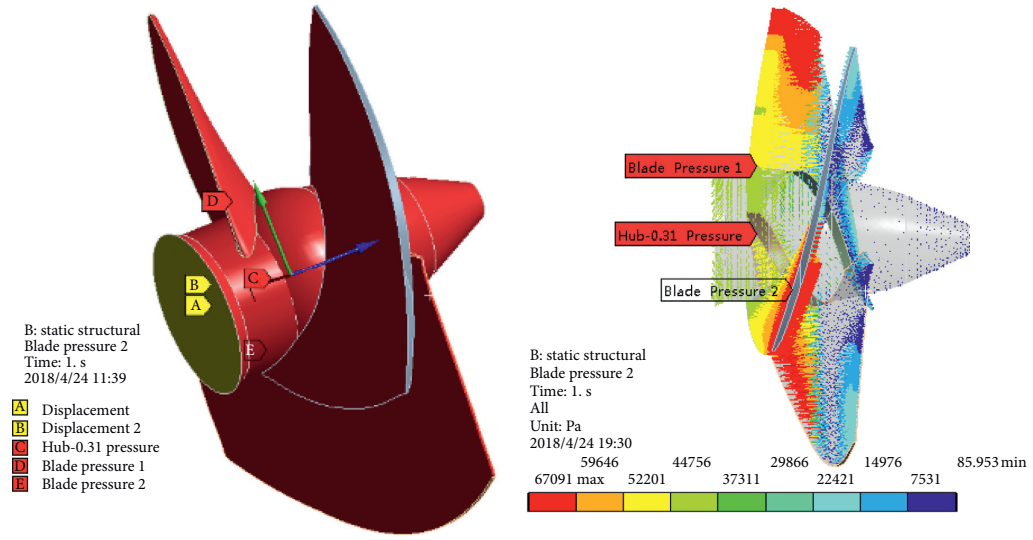

(a) (b)

Figure 8: The boundary conditions of structural field: (a) boundary conditions; (b) water pressure loading.

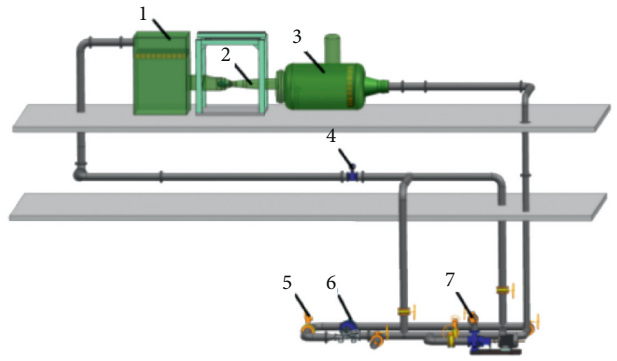

1. Pressure tank
2. Model turbine
3. Tail tank
4. Electromagnetic flowmeter
5. The electromagnetic valve
6. Water supply pump
7.Filling pump

Figure 9: Schematic diagram of the three-dimensional model of the multifunctional test stand.

Figure 10: Photo of the multifunctional test rig.

Table 5: Comparison of numerical simulation calculation and test results under different working conditions.

Working condition	n_{11}/r/min	Q_{11}/m^3/s	Guide vane opening/°	Blade angle/°	Effectivenessη/%	
					Calculated	Test value
1	179.0	1.38	48.0	15.0	80.53	78.12
2	169.8	1.65	52.0	20.3	84.87	82.50
3	170.6	2.01	56.1	25.3	90.79	88.36
4	190.0	2.84	68.0	33.5	89.92	87.25
5	180.0	3.20	71.5	38.6	85.56	83.01
6	187.6	3.52	73.7	39.8	81.71	79.37

Table 6: Calculation results of various design schemes.

Plan	Judgment index				
	Effectiveness η/%	Output P/kW	Pressure pulsation coefficient C_P	Maximum deformation of blade/mm	Maximum static stress of blade/MPa
1	71.34	1727.41	4.4510	1.62	20.25
2	80.53	2576.65	1.1472	1.44	24.20
3	91.02	3127.65	0.7879	0.99	27.07
4	84.57	3087.91	1.1761	1.04	26.79
5	85.92	2982.89	0.6178	3.05	50.25
6	87.78	3297.23	1.1185	0.91	26.12
7	75.19	1940.22	7.9660	1.67	20.41
8	80.59	2768.03	2.1571	1.17	22.09
9	86.98	3185.20	2.6395	1.02	25.26
10	83.16	2934.21	2.4201	0.74	19.47
11	79.90	2266.58	1.3565	0.96	27.21
12	75.19	1926.01	1.4233	2.95	27.38
13	72.49	1977.54	3.9701	1.22	20.76
14	70.04	1172.33	2.4499	3.01	27.38
15	88.83	3079.09	1.0581	0.87	22.16
16	85.78	2948.61	0.7246	0.97	21.25

Table 7: Intuitive analysis of the better solution.

Evaluation indexes	Efficiency	Output	Pressure pulsation coefficient	Deformation of blade	Static stress of blade
Plan	3	6	5	10	10
Factor level	$A_1B_3C_3D_3E_3$	$A_2B_2C_1D_4E_3$	$A_2B_1C_2D_3E_4$	$A_3B_2C_4D_3E_1$	$A_3B_2C_4D_3E_1$
Better plan	(a)	(b)	(c)	(d)	(e)

blade's work effectively. Therefore, it is crucial to choose the appropriate distance between the guide vane and blade for the unit's operation.

5.3.3. Influence of Wheel Hub Ratio d (Factor C). It can be seen from Figure 11 that when the hub ratio d changes from $0.29 \longrightarrow 0.31 \longrightarrow 0.33 \longrightarrow 0.35$, the efficiency and output of the corresponding bulb tubular turbine unit increase first and then decrease, and the pressure pulsation coefficient decreases first and then increases. When $d = 0.31$, the unit efficiency and output are the largest, and the pressure pulsation coefficient is the smallest. Reducing the hub ratio helps reduce the hydraulic friction loss of the flow passage components, increase the flow rate, and thereby improve the efficiency of the turbine. Simultaneously, it can save the manufacturing materials of the hub. But if the hub ratio is too small, the blade will be too twisted, leading to turbulent flow and reducing the efficiency of the unit [30]. When the hub ratio gradually increases, the blade deformation and blade static stress values both increase and then decrease. When $d = 0.31$, the blade deformation and stress values are the largest, showing that the selection of hub ratio should take into account the requirements of structural strength and hydraulic performance.

5.3.4. Influence of Blade Relative Twist Angle $\triangle\beta 0$ (Factor D). It can be seen from Figure 11 that the blade relative torsion angle $\triangle\beta_0$ has the most obvious effect on the unit's operating efficiency and output. As the blade relative torsion angle increases, the efficiency and output gradually increase, and the rate increases when $\triangle\beta_0$ is small. The change of the blade relative torsion angle also significantly influences the pressure pulsation coefficient. When $\triangle\beta_0$ increases from 20° to 30.5°, the pressure pulsation coefficient decreases

significantly and then increases slowly. Besides, the blade deformation is affected by the blade relative twist. When $\triangle\beta_0 = 30.5^\circ$, the blade deformation is the smallest, but when $\triangle\beta_0 = 27^\circ$, the stress value is the smallest. It can be concluded that increasing the relative twist angle of the blade can increase the runner's flow capacity, improve the flow pattern of the unit, and reduce the deformation of the blade. However, when the blade's relative twist angle is too large, the blade is difficult to process, and the processing technology is difficult to guarantee.

5.3.5. Influence of Cascade Density l/t (Factor E). It can be seen from Figure 11 that the change of the cascade density has little effect on the efficiency and output of the unit. However, it significantly affects the pressure pulsation coefficient, blade deformation, and blade static stress. When the cascade density l/t increases from 0.72° to 0.84°, the pressure pulsation coefficient increases first and then decreases, and the blade deformation and blade static stress are gradually increased. It can be concluded as follows.

When the cascade's density is small, the flow capacity of the runner is large, the friction area is small, and the unit's efficiency is improved. When the cascade density is large, the stress area of the blade increases, and the deformation and stress value of the blade increase, which requires the increase of blade strength and stiffness.

Through the range analysis, the better schemes obtained are (f), (g), (h), (i), (j), as shown in Table 8.

From the magnitude of the range R, we can see that the significance order of the five factors on the evaluation index is as follows: the efficiency is $D > B > C > A >$ E. The output is $D > A > E > B >$ C. The pressure pulsation coefficient is $D > C > E > B >$ A. The amount of blade deformation is $D > C > E > B >$ A. The static stress value of the blade is $E > C > A > D >$ B.

5.4. Comprehensive Frequency Analysis. The five evaluation indexes of this orthogonal experiment are of equal importance. According to the better plan obtained by intuitive analysis and the better plan obtained by range analysis, a comprehensive frequency analysis of each factor is performed, as shown in Table 9.

It can be seen from the table that level 2 of factor A, level 3 of factor B, level 2 of factor C, level 3 of factor D, and level 1 of factor E occur most frequently. Therefore, the optimal solution was determined to be A2B3C2D3E1. The specific parameters were as follows: the number of guide vanes was 16, the distance between guide vanes and blades was 1995 mm, the hub ratio was 0.31, the relative twist angle of the blades was 27°, and the cascade density was 0.72.

6. Comparative Analysis of Optimization Plans

The following focuses on comparing the calculation results of the steady flow characteristics, unsteady flow characteristics, and unidirectional fluid-solid coupling of the bulb tubular turbine with the flow rate of 0.38Qr under low flow conditions before and after optimization.

6.1. Steady Flow Analysis. After optimization, the unit's small flow conditions' efficiency increases from 86.01% to 90.93%, an increase of 5.72%, and the output increases from 1234.10 kW to 1269.42 kW, an increase of 2.86%. It can be concluded that the optimal scheme obtained through orthogonal test optimization can effectively improve the operating performance of the bulb tubular turbine unit.

Figure 12 is the pressure and streamline diagram of the flow passage section at $X = 0$ before and after optimizing the unit under low flow conditions. It can be seen that the streamline of the inlet flow channel is better than before. Before optimization, there are many obvious vortex zones at the draft tube, and there are different degrees of backflow and vortex zones. After optimization, the optimized draft tube has reduced vortices, and the flow pattern is smooth. Before the optimization, there is an obvious high-pressure area. The pressure difference between the front and back of the blade is large, and cavitation is easy to occur. The optimized pressure is uniform. The cavitation performance is better, indicating that the pressure difference between the optimized inlet and outlet channel is greater than that before optimization, conducive to the positive flow of water, and helps work on the unit.

Figure 13 shows the distribution of blade surface pressure and streamlines before and after optimization. It can be seen that before optimization, there is a significant backflow phenomenon on the front of the blade, and there is a vortex on the back of the blade, and the flow pattern is poor. After optimization, the flow pattern on the front and back of the blade is significantly improved, the vortex on the back of the blade disappears, and the streamlines are smooth. Before optimization, there exists obvious low-pressure area at the front edge of the blade and at the rim of the blade's inlet side, which is prone to cavitation. After optimization, the pressure distribution on the front and back of the blade is more uniform. The area of the low-pressure area is reduced or even disappeared, and the cavitation phenomenon is reduced. It shows that the optimized blade has better work performance and good cavitation performance.

The thickness of the blade gradually decreases from the hub to the rim. The three cross-sections are evenly taken in the blade's circumferential direction to analyze and optimize the change of the blade's surface pressure from the hub to the rim. The cross-sections' distribution positions from the hub to the rim are span = 0.25, span = 0.50, and span = 0.75. The specific cross-sectional position is shown in Figure 14.

Figure 15 shows the static pressure distribution on the blade surface before and after optimization. From the theoretical knowledge of hydraulic turbines, the blade's front and back pressure determine the blade's energy exchange. The greater the pressure difference between the front and back, the greater the blade's torque, the higher the efficiency of energy exchange.

From Figure 15, the area of the low-pressure area on the back of the blade after optimization is reduced, indicating that the optimized blade's cavitation performance becomes better. The reason is as follows: the pressure on the front and back of the blade changes in the radial gradient after optimization becomes smaller; the gradient distribution is

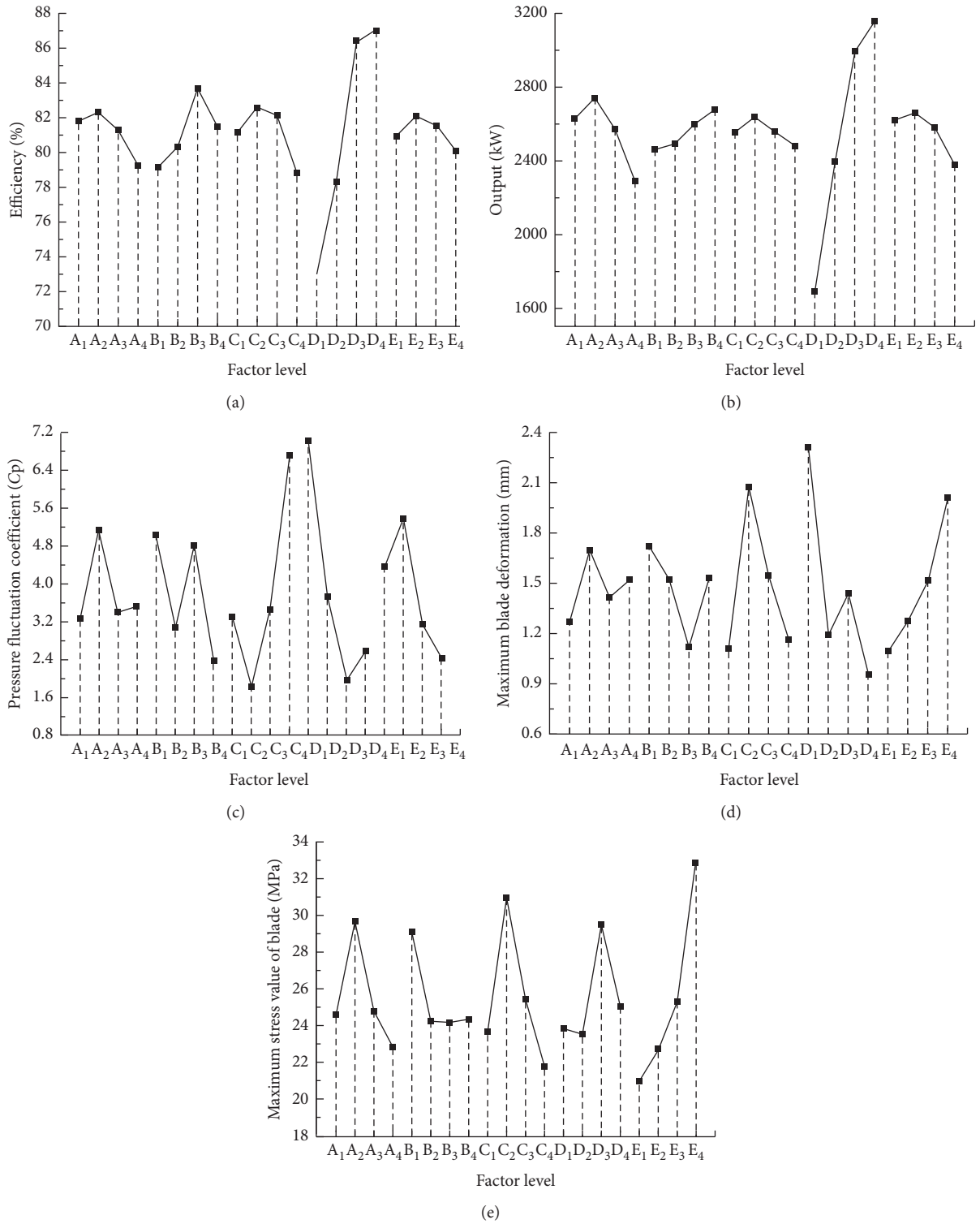

Figure 11: The relationship between various factor levels and indicators: (a) efficiency index; (b) output index; (c) pressure coefficient index; (d) blade deformation index; (e) blade static stress index.

Table 8: The better solution of range analysis.

Evaluation indexes	Efficiency	Output	Pressure pulsation coefficient	Blade deformation	Blade static pressure value
Factor level	$A_2B_3C_2D_4E_2$	$A_2B_4C_2D_4E_2$	$A_1B_4C_2D_3E_4$	$A_1B_3C_1D_4E_1$	$A_4B_3C_4D_2E_1$
Better plan	(f)	(g)	(h)	(i)	(j)

Table 9: Frequency table of each factor level.

Factor level	A_1	A_2	A_3	A_4	B_1	B_2	B_3	B_4	C_1	C_2	C_3	C_4	D_1	D_2	D_3	D_4	E_1	E_2	E_3	E_4
Frequency	3/10	2/5	1/5	1/10	1/10	3/10	2/5	1/5	1/5	2/5	1/10	3/10	0	1/10	1/2	2/5	2/5	1/5	1/5	1/5

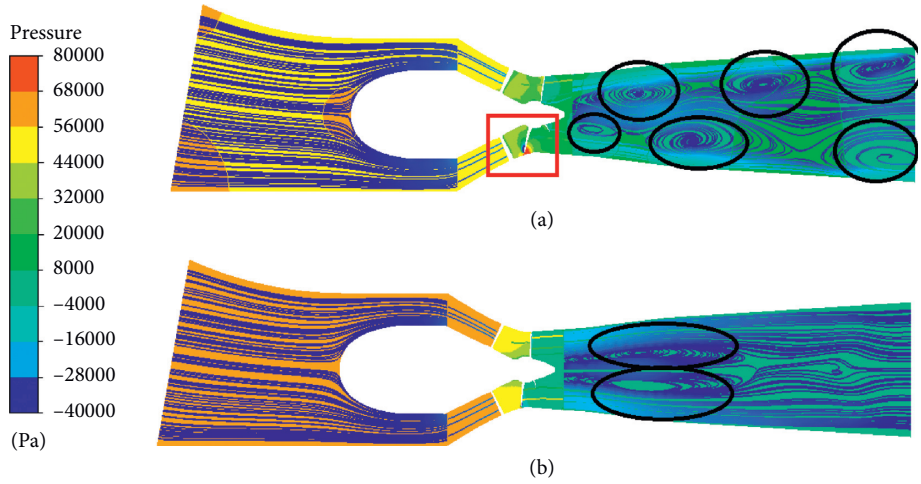

Figure 12: Streamline pressure diagram of $X = 0$ cross-section full flow channel before and after optimization: (a) before optimization; (b) optimized.

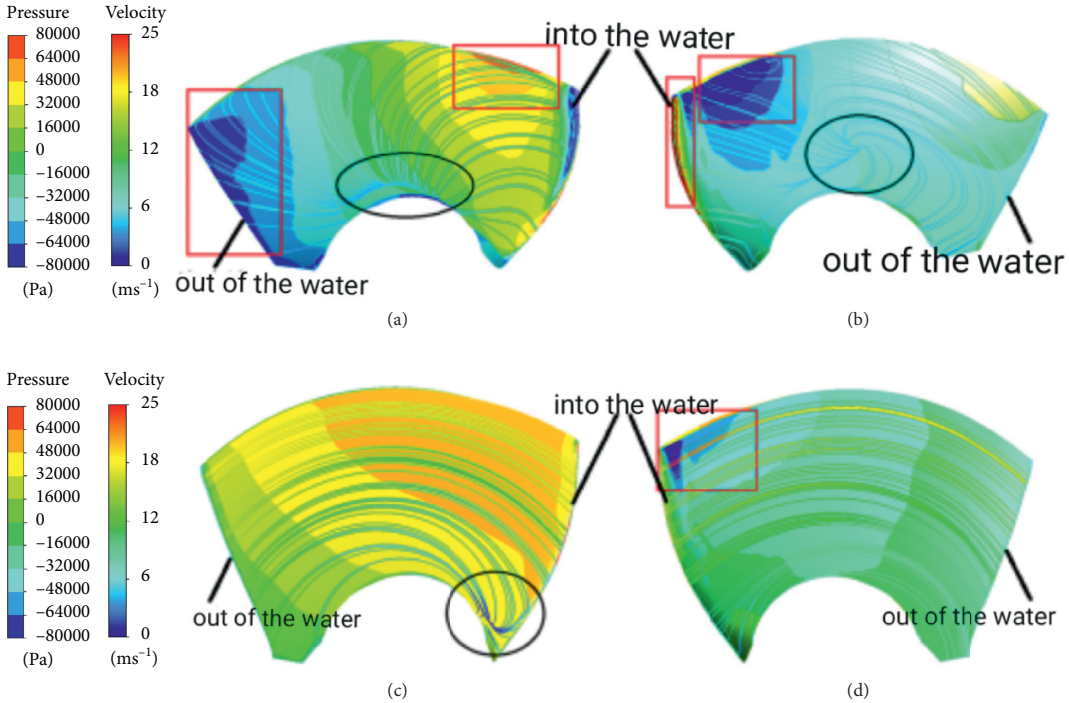

Figure 13: Blade surface pressure and streamline diagram: (a) blade front before optimization; (b) blade back before optimization; (c) optimized blade front; (d) optimized blade back.

more uniform, and the pressure difference between the front and back of the blade is larger than before the optimization.

6.2. Unsteady Flow Analysis. Table 10 shows the main frequency and maximum amplitude of pressure pulsation at the monitoring points at the guide vane inlet, runner inlet,

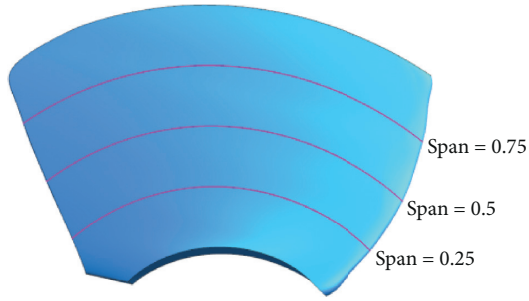

Figure 14: Location of blade cross-section.

runner outlet, and draft tube before and after unit optimization. It can be seen from the table that for small flow conditions, before and after optimization, the runner is subjected to the impact of water flow to generate a vortex rope, and there is dynamic and static interference between the guide vane and the runner. Therefore, the pressure pulsation amplitude at the monitoring point at the runner entrance is the largest, and the frequency is the blade passing frequency 3 fn.

Before optimization, the main frequency at the runner outlet is 3 fn, and the pressure pulsation amplitude is large. After optimization, the pressure pulsation amplitude at the monitoring point at this location is significantly reduced. The main frequency becomes 0.167 fn, indicating that the flow pattern is better when the optimization scheme is selected and the vortex is reduced. At this time, the runner outlet is more affected by the low-frequency pulsation of the draft tube.

After the unit is optimized, the maximum amplitude of pressure pulsation is significantly reduced, especially at the runner entrance, which is reduced by 73.15%, and the stability is improved.

Figure 16 is the pressure pulsation diagram of the monitoring point at the runner entrance in the runner before and after optimization under low flow conditions. It can be seen from Figures 16(a) and 16(c) that before and after optimization, the pressure pulsations at monitoring points B1 and B2 fluctuate less in the time domain. The pressure pulsations at monitoring points B3 and B4 are the domain and have the same periodicity; that is, there are three obvious peaks and troughs in a period in a calculation, the number of which is the same as the number of blades, and the amplitude of fluctuation after optimization is reduced compared with that before optimization. It can be seen from Figures 16(b) and 16(d) that the main frequency of the pressure pulsations at the monitoring points B1 to B4 is 3fn. The blade passing frequency and the amplitude of the pressure pulsation at the monitoring point from the hub to the rim gradually increase, indicating that the flow pattern at the rim is poor. After optimization, the pressure pulsation amplitude at the inlet of the runner drops significantly, indicating that this optimization scheme can reduce the pressure pulsation amplitude in the flow paasage and improve the unit's stability.

6.3. Unidirectional Fluid-Solid Coupling Analysis. The structural stress and deformation of the runner blades before and after the orthogonal test optimization are compared and analyzed through one-way fluid-solid coupling calculation. Figures 17 and 18 are the blade deformation distribution diagram and static stress cloud diagram before and after optimization.

It can be seen from Figure 17 that before and after optimization, the deformation of the outlet side of the blade is small, and the deformation mainly occurs at the inlet side of the blade. The deformation of the inlet side gradually increases from the hub to the rim.

From Figure 18, before and after optimization, the runner structure's maximum static stress appears at the root of the blade inlet. The distribution of static stress along the blade decreases with increasing radius. After optimization, the gradient of static stress change is more obvious, and the stress value becomes small. The blade's structure and the hub can be regarded as a cantilever beam, the connection is the fixed end, and the other end is the free end. After the surface pressure load is applied, the deformation at the fixed end is zero, the bending moment is the largest, and the static stress is the largest. While the bending moment at the free end is zero, the static stress is the smallest, and the deformation is the largest; the stress on the inlet side is larger than the outlet side, so its deformation is also larger than the outlet edge.

After the turbine unit's optimization, the maximum deformation value of the blade is reduced from 1.0754 mm to 0.64971 mm, a decrease of 39.59%; the maximum static stress value of the blade is reduced from 26.130 MPa to 22.691 MPa, a decrease of 13.16%. It can be seen that the optimal scheme obtained by the orthogonal test improves the structural strength of the runner part of the bulb tubular turbine.

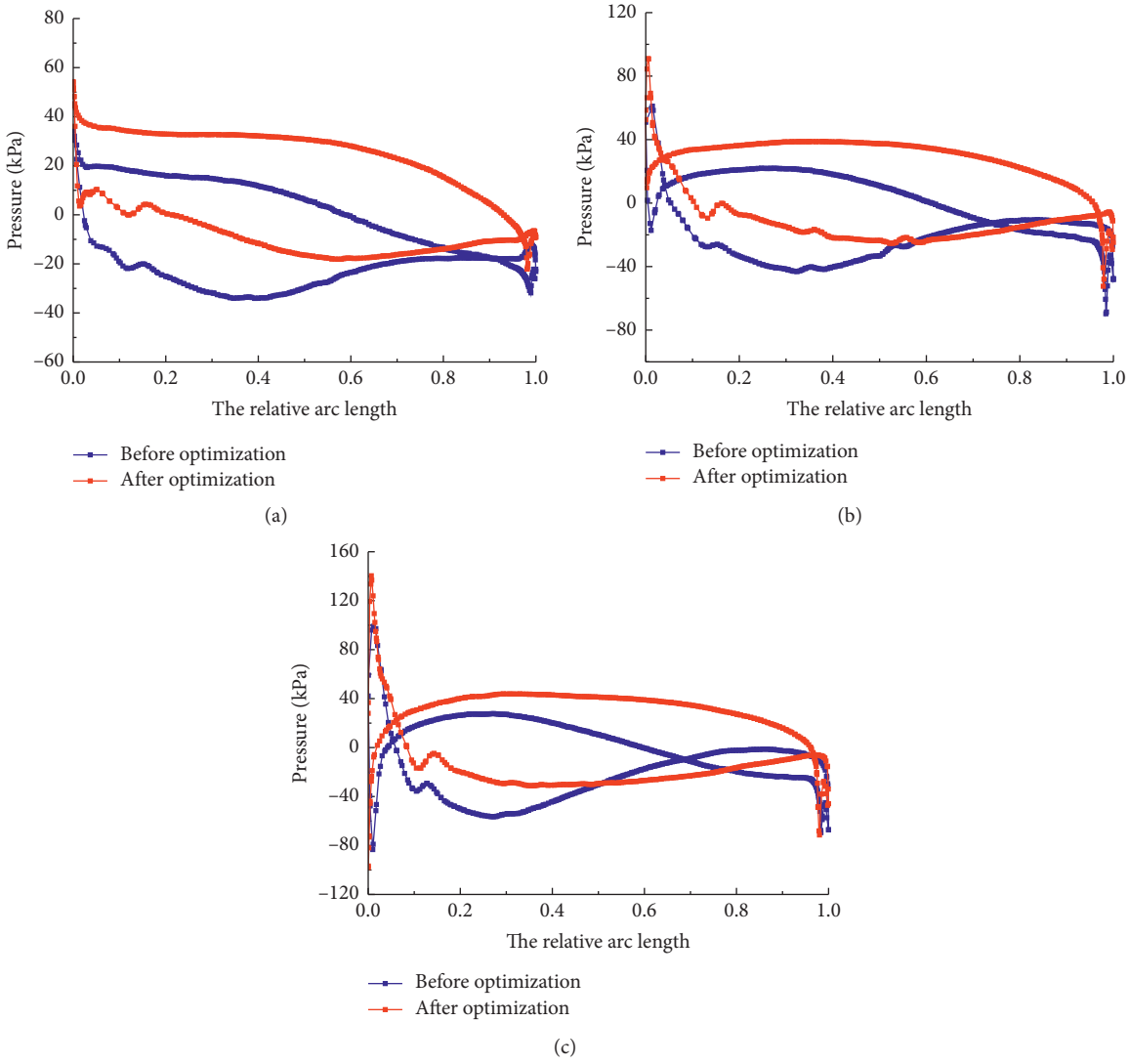

Figure 15: Static pressure distribution on the blade surface before and after optimization: (a) span = 0.25; (b) span = 0.5; (c) span = 0.75.

Table 10: Maximum amplitude of pressure pulsation at each monitoring point before and after optimization.

Monitoring points		A1–A4	B1–B4	C1–C4	D1–D4
Before optimization	Frequency/Hz	3 fn	3 fn	3 fn	0.167 fn
	Amplitude/%	0.591	5.121	1.741	0.656
Optimized	Frequency/Hz	3 fn	3 fn	0.167 fn	0.167 fn
	Amplitude/%	0.308	1.375	0.512	0.484

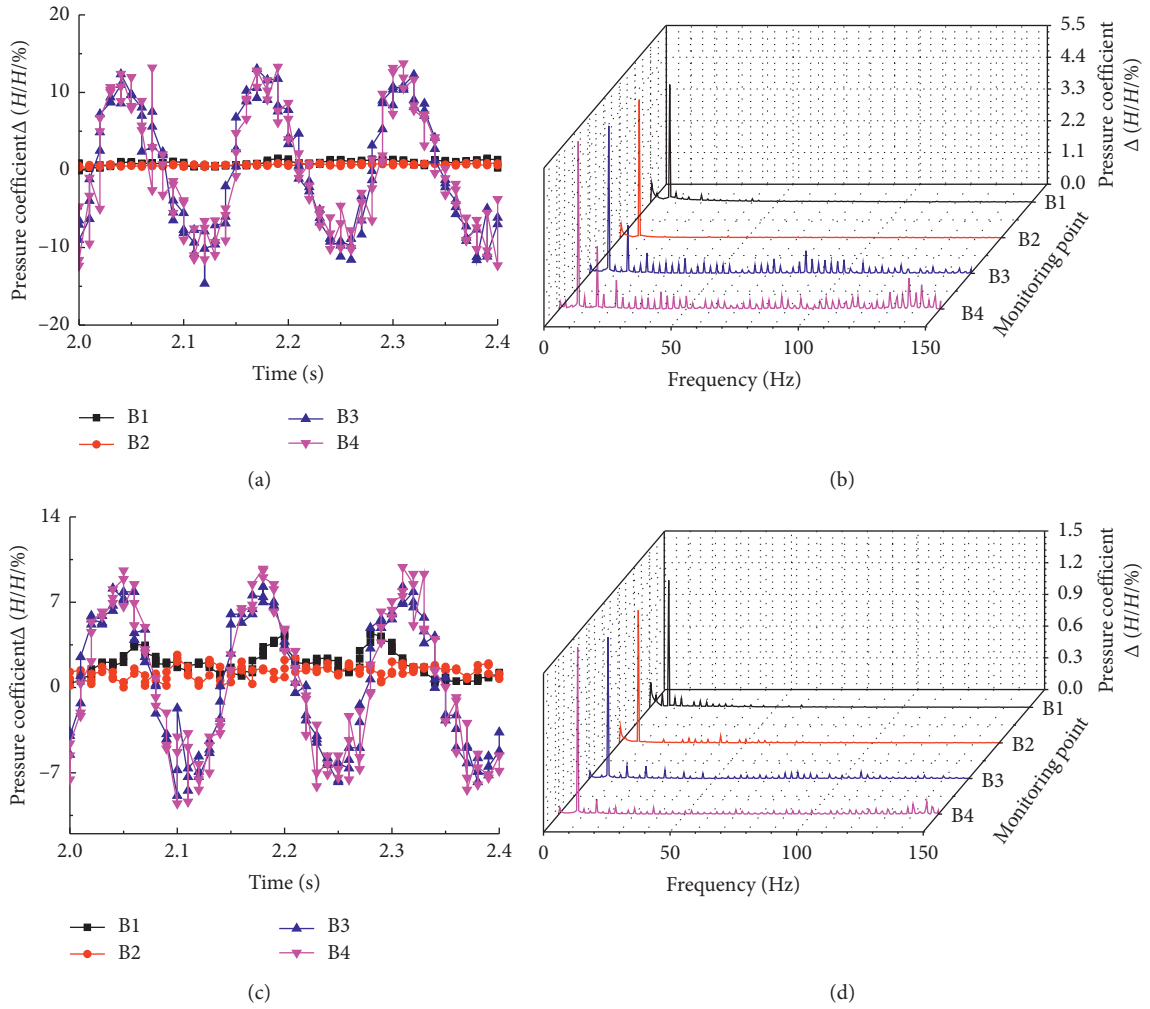

Figure 16: Optimization of pressure pulsation at the inlet and outlet monitoring points of the runner: (a) time-domain graph before optimization; (b) frequency domain graph before optimization; (c) time-domain graph after optimization; (d) optimized frequency domain graph.

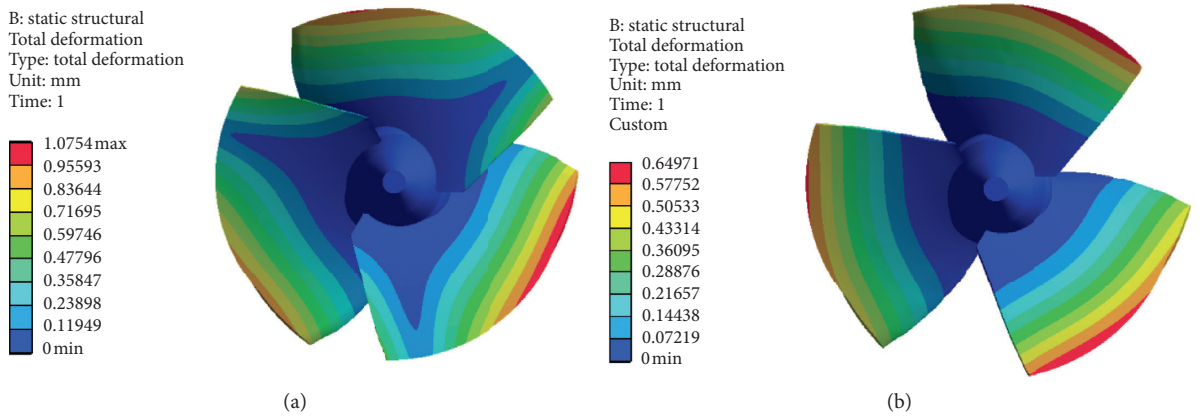

Figure 17: Distribution of blade deformation before and after optimization: (a) before optimization; (b) optimized.

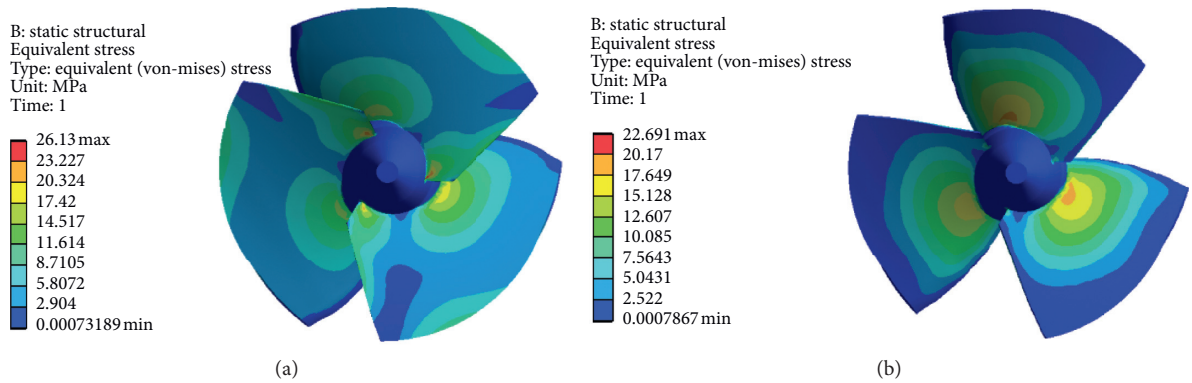

Figure 18: Static stress cloud of the blade before and after optimization: (a) before optimization; (b) optimized.

7. Conclusion

In this article, the orthogonal test method is used to optimize the multiobjective bulb turbine. The five indexes of unit efficiency, output, pressure pulsation, blade deformation, and blade static stress are used as judgment criteria, revealing the impact of these five factors (number of guide vanes, the distance between the guide vanes and the blades, hub ratio, blade relative torsion angle, and cascade density) on the hydraulic performance, operating stability, and structural strength of the bulb tubular turbine. The performance of the turbine before and after the optimization is compared and analyzed. The conclusion is as follows:

(1) The optimal scheme of bulb tubular turbine is as follows: the number of guide vane is 16, the distance between guide vane and the blade is 1995 mm, the hub ratio is 0.31, the relative twist angle of the blade is 27°, and the cascade density is 0.72.

(2) Range analysis shows that blade relative torsion angle is an important geometric parameter in the hydraulic design of bulb tubular turbine. The number of guide vanes mainly affects the unit output; the distance between guide vane and blade mainly affects efficiency; hub ratio mainly affects pressure pulsation and blade deformation; cascade density mainly affects blade static stress. The relative twist angle change of the blade has the most significant influence on the four test evaluation indexes except the blade's static stress.

(3) After optimization, the hydraulic performance, stability, and structural strength of the unit are all improved, verifying the feasibility of the integrated frequency analysis method in the multiobjective orthogonal test of bulb tubular turbine. After optimization, the bulb tubular turbine's efficiency and output are increased by 5.72% and 2.86% at a low flow rate, respectively. The vortex at the tailpipe is reduced, and the cavitation performance is well. The maximum pressure pulsation amplitude in the flow passage is reduced by 73.15%, the maximum blade deformation is reduced by 39.59%, and the maximum blade static stress is reduced by 13.16%.

(4) The numerical simulation results are consistent with the model test data, and the error is within ±3%, which verifies the reliability of the numerical simulation calculation, indicating that the numerical calculation model and method used in this article can more accurately predict the performance of the bulb tubular turbine. In future work, the turbulence model's optimization to further reduce the error is worthy of the effort. Moreover, the analysis and comparison of different design optimization methods should be the focus of the research.

Data Availability

No data were used to support this study.

Conflicts of Interest

The authors declare that they have no conflicts of interest.

Acknowledgments

The project was supported by the Central University Fundamental Research Funds (2015B02814) and the IWHR Research and Development Support Program (HM0145B182017).

References

[1] Z. T. Liang and B. C. Hu, "Discussion on the application and technique development of tubular turbine in China," *China Rural Water And Hydropower*, no. 6, pp. 91-92 + 95, 2005.

[2] Z. Liu, S. Y. Zou, J. Y. Li et al., "Reason analysis and countermeasures research for output deficiency of bulb turbines," *Power System Engineering*, vol. 30, no. 6, pp. 73-74, 2014.

[3] F. Zhang, J. F. Chen, G. Lu et al., "Output power improvement research of bulb turbine," *Journal of China Institute of Water Resources and Hydropower Research*, vol. 14, no. 3, pp. 219–223, 2016.

[4] L. Wu and H. C. Pan, "Simulation of flow fields in a hydro turbine used for tidal hydropower stations," *Mechanical&-Electrical Engineering Magazine*, vol. 27, no. 10, pp. 21–24, 2010.

[5] Z. W. Wang, L. J. Zhou, Y. G. Chen et al., "Hydraulic loss analysis in bulb turbine," *Large Electric Machine And Hydraulic Turbine*, no. 5, pp. 40–43, 2004.

[6] L. Bai, L. Zhou, X. Jiang, Q. Pang, and D. Ye, "Vibration in a multistage centrifugal pump under varied conditions," *Shock and Vibration*, vol. 2019, Article ID 2057031, 9 pages, 2019.

[7] Y. Yang, L. Zhou, W. Shi, Z. He, Y. Han, and Y. Xiao, "Interstage difference of pressure pulsation in a three-stage electrical submersible pump," *Journal of Petroleum Science and Engineering*, vol. 196, Article ID 107653, 2020.

[8] S. Tang, S. Yuan, and Y. Zhu, "Deep learning-based intelligent fault diagnosis methods toward rotating machinery," *IEEE Access*, vol. 8, no. 1, pp. 9335–9346, 2020.

[9] Y. Yang, L. Zhou, J. Hang, D. Du, W. Shi, and Z. He, "Energy characteristics and optimal design of diffuser meridian in an electrical submersible pump," *Renewable Energy*, vol. 167, pp. 718–727, 2021.

[10] L. H. Wang, L. Z. Han, and J. D. Wang, "Study on the affect of the cascade solidity to the efficiency of tubular turbine," *Large Electric Machine And Hydraulic Turbine*, vol. 29, no. 5, pp. 48–50, 2006.

[11] Y. P. Zhao, W. L. Liao, Z. H. Li et al., "Flow field performance of bulb turbine with C-type or S-type blades," *Transactions of the Chinese Society of Agricultural Engineering*, no. 17, pp. 47–53, 2013.

[12] W. Yang, Y. Wu, and S. Liu, "An optimization method on runner blades in bulb turbine based on CFD analysis," *Science China Technological Sciences*, vol. 54, no. 2, pp. 338–344, 2011.

[13] Z. G. Li, X. Z. Wei, F. C. Li et al., "Based on turbine inlet flow angle of tubular turbine optimal working conditions research and apply," *Transactions of the Chinese Society of Agricultural Engineering*, vol. 31, no. 14, pp. 83–89, 2015.

[14] F. C. Li, H. G. Fan, Z. W. Wang et al., "Three-dimensional matching design method for runner blades and guide vanes of tubular turbine," *Journal Of Hydroelectric Engineering*, vol. 29, no. 4, pp. 213–218, 2010.

[15] Y. Zheng, L. Y. Li, D. Q. Zhou et al., "Joint design of supports and guide vanes in micro head bulb turbine," *Journal of Huazhong University of Science and Technology (Nature Science Edition)*, vol. 42, no. 9, pp. 128–132, 2014.

[16] Y. T. Kim, S. H. Nam, Y. J. Cho et al., "Tubular-type hydroturbine performance for variable guide vane opening by CFD," *New Trends in Fluid Mechanics Research*, Springer, Berlin, Germany, 2009.

[17] C. Kang, L. T. Li, and G. H. Lu, "Influence of guide vane opening on performance and flow characteristics of tubular hydro-turbine," *Journal of Drainage and Irrigation Machinery Engineering*, vol. 34, no. 5, pp. 406–413, 2016.

[18] Y. Zheng, A. R. Sun, C. X. Yang et al., "Multi-objective optimization design and test of axial-flow pump," *Transactions of the Chinese Society for Agricultural Machinery*, vol. 48, no. 9, pp. 129–136, 2017.

[19] X. F. Gao, W. D. Shi, D. S. Zhang et al., "Optimization design and test of vortex pump based on CFD orthogonal test," *Transactions of the Chinese Society for Agricultural Machinery*, vol. 45, no. 5, pp. 101–106, 2014.

[20] Y. L. Li, L. Yu, X. B. Zhou et al., "Parameters sensitivity analysis of successive dam break model for cascade reservoir based on the orthogonal test method," *Journal of Hydraulic Engineering*, vol. 49, no. 7, pp. 823–830, 2018.

[21] S. B. Xing, R. S. Zhu, D. X. Zhu et al., "Axial-flow pump optimization design based on the orthogonal experiment," *China Rural Water and Hydropower*, no. 1, pp. 167–171, 2015.

[22] T. S. Xu, *Orthogonal Test based on Object-Oriented Finite Element Program Design and its Research in Structural Optimization*, Jilin University, Changchun, China, 2009.

[23] Z. C. Shi, *Expermental Research and Orthogonal Experiment Design of Urination Assist System Driven by Ultrasonic-Vaporized Steam*, Guangdong University of Technology, Guangzhou, China, 2014.

[24] S. T. Tian, *Practical Technology of Tubular Turbine Generator Set—Design Construction and Installation Operation and Maintenance (First volume)*, China Water Power Press, Beijing, China, 2010.

[25] Y. L. Wu, J. Liu, T. J. Chen et al., *Vane Pump Design and Examples*, Mechanical Industry Press, Beijing, China, 2011.

[26] B. Quatember and H. Mühlthaler, "Generation of CFD meshes from biplane angiograms: an example of image-based mesh generation and simulation," *Applied Numerical Mathematics*, vol. 46, no. 3-4, pp. 379–397, 2003.

[27] F. X. Zhang, Y. Zheng, J. F. Wei et al., "Stress analysis of tubular turbine based on fluid-structure coupling," *Journal of Hydroelectric Engineering*, vol. 33, no. 3, pp. 267–273, 2014.

[28] G. J. Zhu, X. Q. Luo, J. J. Feng et al., "Variable coupling strength analysis of Francis turbine runner design," *Transactions of the Chinese Society of Agricultural Engineering*, vol. 33, no. 22, pp. 36–45, 2017.

[29] Y. Zheng, W. Q. Jiang, Y. J. Chen et al., "Investigation on low frequency pulsating and draft tube vortex of tubular turbine," *Transactions of the Chinese Society for Agricultural Machinery*, vol. 49, no. 4, pp. 165–171, 2018.

[30] Y. Zheng, L. Li, H. X. Chen et al., "Influence of hub ratio on hydraulic performance and structural strength of bulb tubular turbine," *Journal of Hydraulic Engineering*, vol. 49, no. 10, pp. 1303–1311, 2018.